Journal of Materials Chemistry B

ROYAL SOCIETY OF CHEMISTRY

PAPER

View Article Online
View Journal

Cite this: DOI: 10.1039/d6tb00438e

Dictated cell adhesion and migration using microfluidic-controlled synthetic hydrogels exhibiting programmable viscoelasticities

Haochen Yang,[a] Ziyuan Li,*[a] Gilad Davidson-Rozenfeld,[c] Meng Li,[a] Yuxing Shang,†[b] Linjie Chen,[a] Yingchao Ma,[a] Yifan Ge,*[b] Itamar Willner *[c] and Junji Zhang *[a]

Mechanosensing interactions between the extracellular matrix (ECM) and the intracellular cytoskeleton are fundamental to cellular functions such as motility, proliferation, and adhesion, driven by the dynamic, bidirectional, tension-regulated maturation of focal adhesion (FA) sites. We demonstrate that native mechanosensing interactions and their downstream functions are precisely controlled using synthetic hydrogels. We introduce a microfluidic-assisted synthesis of imine-crosslinked hyaluronic acid-gelatin copolymer hydrogels (HAG), enabling controlled, predefined gradient viscoelasticity. Specifically, three native tissues (muscle, epidermis, and cartilage)-mimicking HAG hydrogels were prepared, matching their effective Young's modulus (Ymod) and stress relaxation time ($\tau_{1/2}$). Enhanced cell spreading and directional cell migration are observed, with a preference for substrates with tissue-matching viscoelasticity. These mechanosensing reactions are confirmed by traction force microscopy, revealing a tight correlation between native tissue mechano-properties and the hydrogel viscoelastic parameters. We demonstrate that the signaling efficacies of the FAK and associated YAP/TAZ pathways, central regulators of FA formation and cell migration, are tuned by substrate tissue-matching viscoelasticity. We implement these preprogrammed viscoelastic gradient hydrogels as spatiotemporal cell-separation matrices, enabling viscoelasticity-driven migration of binary cell mixtures. This work provides a potent platform for studying cell-material interactions, offering significant potential applications in tissue engineering, immunotherapy, and regenerative medicine.

Received 25th February 2026,
Accepted 23rd April 2026

DOI: 10.1039/d6tb00438e

rsc.li/materials-b

1. Introduction

The interactions between the intracellular skeleton and the extracellular matrix (ECM) orchestrate diverse physiological and pathological processes such as embryogenesis, homeostasis, cancer progression, tissue repair, and wound healing.[1–4] The primary interactions of the transmembrane-embedded integrin with the ECM result in the counter-bridged binding of the cytoskeleton to the integrin, resulting in the ECM-dictated adaptive rearrangement of the cytoskeleton (actomyosin fibers) complexes, sensing the traction force induced by the fibers, and the restoring stress exerted by the ECM-bound integrin.[5–8] The mechanosensing functions of the cells are, then, translated into mechanotransduction signaling of cell functions.[9–11] These are reflected by downstream phosphorylation/dephosphorylation YAP/TAZ-mediated transformations leading to motility, proliferation, and adhesion functions.[12–14] Concomitantly, the mechanosensing ECM-induced interactions lead to adaptive focal adhesion (FA) sites controlled by the bidirectional, tension-regulated, mechanosensing interactions with the ECM.[15,16] For tight cell-ECM interactions, the recruitment of YAP/TAZ-mediated intracellular proteins stabilizing the FA site proceeds (FA maturation), whereas weak cell-ECM interactions lead to inhibited FA sites.[17,18] That is, the bidirectional mechanosensing cell-ECM interactions control intracellular signaling and mechanical cell behavior.[3,19–21]

Substantial research efforts are directed to mirror cell-ECM interactions through biomimetic cell-synthetic hydrogel

[a] Key Laboratory for Advanced Materials and Joint International Research Laboratory of Precision Chemistry and Molecular Engineering, Feringa Nobel Prize Scientist Joint Research Center, Frontiers Science Center for Materiobiology and Dynamic Chemistry, Institute of Fine Chemicals, School of Chemistry and Molecular Engineering, East China University of Science and Technology, Shanghai 200237, China. E-mail: ziyuan.li@ecust.edu.cn, zhangjunji@ecust.edu.cn
[b] Interdisciplinary Research Center on Biology and Chemistry, Shanghai Institute of Organic Chemistry, Chinese Academy of Sciences, Shanghai 201210, China. E-mail: itamar.willner@mail.huji.ac.il
[c] Institute of Chemistry, The Center for Nanoscience and Nanotechnology, The Hebrew University of Jerusalem, Jerusalem 91904, Israel. E-mail: yifange@sioc.ac.cn
† Current address: School of Chemistry and Molecular Engineering, East China Normal University, Shanghai 200241, China.

interactions.[22–25] Diverse methods to synthesize hydrogels of controlled stiffness (and elasticity) were reported.[26–30] The interactions of cells with stiffness-controlled hydrogel matrices were examined, and the links between the hydrogel stiffness and cell behavior were demonstrated.[31–35] Particularly, the gel stiffness-controlled differentiation of stem cells to target cells was demonstrated. For example, stiff hydrogels induced differentiation of stem cells into osteoblasts, whereas lower-stiffness hydrogels induced stem cell differentiation into adipocytes.[36] Moreover, hydrogels exhibiting gradient stiffness demonstrate preferred directional migration (durotaxis) toward higher stiffness.[37–40] These stiffness-controlled cell-ECM reactions were implemented for advanced biomaterial engineering, developing patterned cell arrays,[41–43] wound healing,[44,45] advanced cell therapy platforms,[46,47] robotics,[48–50] and regenerative medicine.[51–53]

Nevertheless, native ECM environments are defined not only by their static elasticities but also influenced by the dynamic viscoelastic properties of the matrices.[54,55] The static elasticity properties of hydrogel substrates are characterized by shear oscillatory rheometry[56,57] and Young's modulus (often measured by indentation methods),[57–59] and the dynamic viscoelastic properties are characterized by rheometry-based static strain application while probing the substrate stress decay. This generates the stress relaxation time, $\tau_{1/2}$, defined as the time interval upon which the stress reaches half of its initial value, indicating how the gel substrate dissipates stress.[56,60–62] Indeed, recent studies emphasized the significance of hydrogel viscosity on cell behavior.[63–65] Time-dependent energy dissipation within the gel matrices leads to a significant effect on the cell behavior, such as cell spreading, morphology, and motility.[66–68] Importantly, native tissues and their interfaces often exhibit gradual transitions in viscoelastic properties rather than discrete, homogeneous mechanical states. Such spatial heterogeneity plays a critical role in regulating cell behavior, particularly at interfacial regions where cells experience continuously varying mechanical cues. However, most existing hydrogel systems are limited to uniform viscoelastic properties, which fail to recapitulate these physiologically relevant gradients. The parallel effects of viscosity and elasticity of hydrogels on cell functions have been scarcely investigated.[69,70] This is mainly due to difficulties in synthesizing hydrogels of programmable, precise viscoelasticity, particularly substrates revealing gradient viscoelasticity.

Here we wish to report on a microfluidic-based method to synthesize precise and reproducible hydrogels exhibiting defined viscoelastic properties and programmable substrates consisting of gradient viscoelastic features. Specifically, we apply the method to synthesize hydrogels consisting of hyaluronic acid/gelatin (HAG),[71–73] revealing programmable and gradient viscoelasticity, and examine the interactions of different kinds of cells with the different synthetic hydrogel substrates. We find that similarly to native cell-ECM interactions, where mechanosensing cell functions are dictated by the viscoelasticity of the ECM, the viscoelasticity of the synthetic gels dictates cell functions. We find that viscoelasticity matching between synthetic hydrogel matrices and the corresponding cell tissue is crucial for controlling cell adhesion and migration on these substrates. The mechanoresponsive behavior of the cells on the respective synthetic matrices and, the mirrored tissue viscoelasticity, are rationalized by cell spreading area evaluation, traction force microscopy imaging, and probing focal adhesion sites by confocal microscopy and immunoblotting experiments. Substrate-dictated directional migration on the gradient viscoelastic hydrogels is demonstrated. The results are applied to highlight the spatial separation of different cell types using predesigned, programmable gradient viscoelastic hydrogel frameworks.

2. Experimental section

All reagents were obtained from commercial sources and used without further purification unless otherwise noted. Essential experimental procedures and supplementary data are provided in the Supporting Information, including materials and instrumentation, preparation and oxidation degree characterization of oxi-HA, fabrication of HAG hydrogels, Fourier transform infrared (FTIR) spectroscopy, scanning electron microscopy (SEM), rheological and nanoindentation measurements, preparation of decellularized matrices, cell culture and cytotoxicity assays, cell migration experiments on viscoelastic gradient substrates, Western blotting, immunofluorescence staining, traction force microscopy, and image analysis.

3. Results and discussion

3.1. Microfluidic-controlled synthesis of hyaluronic acid/gelatin hydrogels exhibiting programmable viscoelasticity

Synthetic hydrogels consisting of imine-crosslinked hyaluronic acid (HA) and gelatin copolymer (HAG) frameworks were prepared, Fig. 1A and Fig. S1, generating complex ECM mimetic matrices. The gel is stabilized by covalent imine bonds, supramolecular H-bonds, and electrostatic interpolymer ion-pairing. The nature of bonds stabilizing the gel enables the synthesis of tunable viscoelastic gels, adjusted by the ratio of the flexible HA and gelatin chains, while balancing the different parameters stabilizing the gels. Fourier transform infrared spectroscopy (FT-IR) confirmed the formation of the HAG hydrogels, where the 1646 cm^{-1} and 1544 cm^{-1} bands of the –C═N, formed between the aldehydes of oxidized HA (HA_{ox}) and –NH of gelatin, Fig. S2. The approach to crosslink HAG hydrogels, which exhibit precisely controlled viscoelasticity, is achieved by automated programmed flow-rate modulation of pregelation solutions containing the HA and gelatin, Fig. 1B. The apparatus used to fabricate the gels enabled a compositional precision of 0.01% (w/v) deposition of the respective droplets, which enabled highly reproducible synthesis of the gradient viscoelastic hydrogels, presenting a major advancement in preparing viscoelastic-gradient gels over conventional fabrication methods, Fig. S3. The capability of the method to generate gels exhibiting tailored viscoelastic gradients (measured by rheometry and nano-indentation) is further demonstrated in Fig. 1C, and Fig. S4–S11, and Tables S1–S3. Accordingly, the gel fabrication methodology enables the tailoring of precise viscoelastic compositional landscapes that offering the generation of

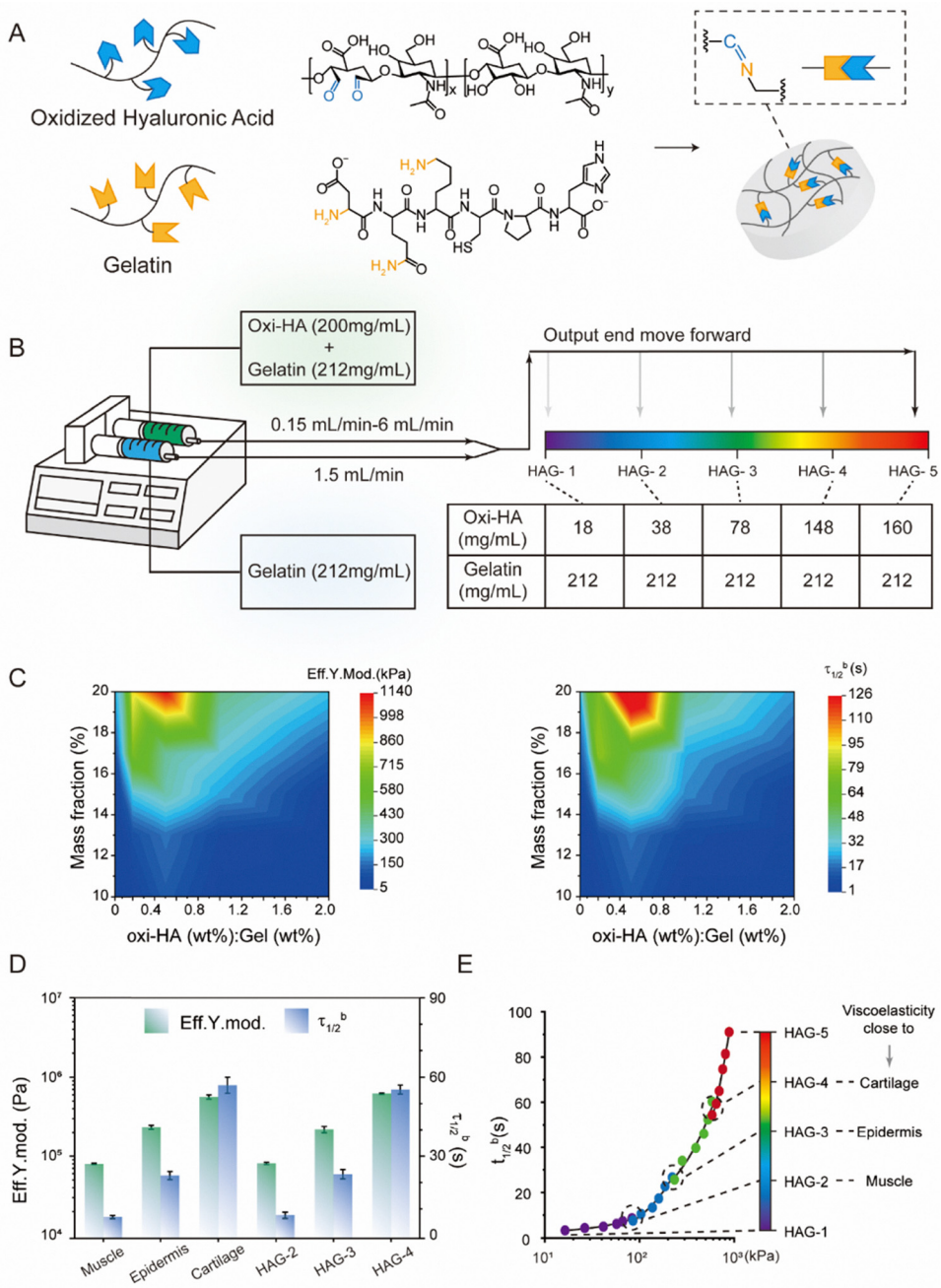

Fig. 1 (A) Schematic structure of the hyaluronic acid (HA)/gelatin crosslinked hydrogel frameworks (HAG). (B) Microfluidic programmable synthesis of HAG framework of gradient viscoelasticity and their programmed composition. (C) Panel I. Effective Young's moduli (Ymod) values mapping a series of HAG frameworks at different HA/gelatin compositions and concentrations. Panel II. A map of stress relaxation time ($\tau_{1/2}$) values of HA/gelatin corresponding to different compositions and concentrations. (D) Effective Ymod and $\tau_{1/2}$ values of distinct biological tissues (muscle, epidermis, and cartilage), and selected HAG gels (HAG-2, HAG-3, and HAG-4) mirroring the effective Ymod and $\tau_{1/2}$ values of the biological tissues. (E) Effective Ymod and $\tau_{1/2}$ values of the microfluidic-controlled synthesized gradient hydrogel consisting of HAG-2, HAG-3, and HAG-4, positioned in between two hydrogels, HAG-1 and HAG-5, exhibiting lower and higher viscoelastic properties.

mechanical dynamic viscoelastic microenvironments presented in native tissues.

3.2. Fabrication of tissue-mimetic viscoelastic hydrogels

The capability to synthesize tailored viscoelastic hydrogel matrices provides a versatile means to prepare viscoelastic gradient hydrogels, overlapping the mechanical features of native tissues. This would allow to probe the effects of the viscoelastic gradient matrices on the cell functions, comprising the tissues, exhibiting overlapping mechanical features.

The mechanical properties of three different types of tissues corresponding to muscle, epidermis, and cartilage were evaluated, and the respective effective Young's modulus values and stress-relaxation ($\tau_{1/2}$) parameters are provided, Fig. 1D.

Moreover, the method to prepare precise viscoelastic gradient gels was adopted to synthesize three gels, HAG-2, HAG-3, and HAG-4, exhibiting viscoelastic properties analogous to the mechanical properties of the tissues, Fig. 1D. That is, the viscoelastic HAG-2 mimics the mechanical properties of muscle tissue, HAG-3 mimics the mechanical properties of epidermis tissue, and HAG-4 mimics the mechanical properties of cartilage tissue. We further synthesized two hydrogels that extend the boundaries of the viscoelastic parameters to lower (HAG-1) and higher (HAG-5) mechanical properties, demonstrated by the set of three tissue-mimicking hydrogels. The successful preparation of the gradient viscoelastic hydrogels was supported by Scanning Electron Microscopy (SEM) analysis, Fig. S12. The pore sizes and densities of the gradient viscoelastic hydrogels are controlled by parameters that govern the different hydrogels. While the gels demonstrating low mechanical parameters show large pore sizes of low density, the gels characterized by higher mechanical viscoelastic parameters demonstrate smaller pore sizes and higher densities. Subsequently, a continuous viscoelastic gradient hydrogel framework, composed of the three hydrogels, framed between hydrogels HAG-1 and HAG-5 was fabricated. Fig. 1E depicts the continuous viscoelastic gradient parameters $\tau_{1/2}$ and Young's modulus across the gel frameworks.

3.3. Directional cell migration and spreading on tissue-mimetic gradient viscoelastic hydrogels

The mechanosensing properties of three types of cells, C2C12 myoblasts, NIH-3T3 fibroblasts, and mouse chondrocytes, were evaluated on the non-linear gradient viscoelastic hydrogel, shown in Fig. 1E, by probing the individual cell migration trajectories and spreading area on the hydrogel substrates exhibiting complex viscoelasticity. The individual migration and spreading area features of the respective cells were probed by analyzing time-lapse microscopy over a time period of 12.5 hours following cell attachment (it should be noted that cytotoxicity assessment of the fabricated hydrogels demonstrated excellent biocompatibility for all three cell lines and well-spread morphology of the cells on the substrates over a time period of 7 days, see Fig. S13). Fig. 2A(i) depicts the mechanosensing behavior of the C2C12 cells, revealing a clear preference towards tissue viscoelasticity corresponding to muscle tissue. Positioning the C2C12 cells at the HAG-1/HAG-2 interface demonstrated, after 12.5 hours, a profound cell migration efficacy towards the HAG-2 gel domain, exhibiting a viscoelasticity of effective Young's modulus of 85 kPa and $\tau_{1/2}$ of 8.3 seconds (while avoiding the softer region HAG-1 characterized by Young's modulus of 18 kPa and $\tau_{1/2}$ of 2.9 seconds). Similarly, positioning of the C2C12 cells at the interface of HAG-2/HAG-3 demonstrated a profound migration efficacy toward the HAG-2 region (while avoiding migration to the stiffer HAG-3 region characterized by a Young's modulus of 230 kPa and $\tau_{1/2}$ of 23.8 seconds), Fig. 2A(ii). In addition, positioning of NIH-3T3 fibroblasts at the interface of HAG-2/HA-G3 reveals migration trajectories preferentially towards the stiffer HAG-3 region, mimicking the epidermis (while avoiding the softer HAG-2), Fig. 2B(i). Positioning the NIH-3T3 cells at the interface between HAG-3/HAG-4 resulted in a preferred migration trajectory towards the softer HAG-3 hydrogel region (while avoiding the stiffer HAG-4 hydrogel region, characterized by a Young's modulus of 654 kPa and $\tau_{1/2}$ of 56 seconds), Fig. 2B(ii). Finally, the positioning of chondrocytes at the interface of HAG-3/HAG-4 demonstrated preferred migration towards the stiffer HAG4 region, mimicking the cartilage tissue (while avoiding the softer HAG3), Fig. 2C(i). Similarly, positioning the chondrocytes at the interface of HAG-4/HAG-5 demonstrated preferred migration towards the softer HAG-4 region (while avoiding the stiffer HAG-5, characterized by a Young's modulus of 856 kPa and $\tau_{1/2}$ of 98 seconds), Fig. 2C(ii). Moreover, control experiments using hydrogels of uniform viscoelastic properties, matching the viscoelasticity of HAG-2, HAG-3, or HAG-4, resulted in non-directional migration patterns of the corresponding cells, Fig. S14. Thus, the gradient viscoelasticity of the substrates, rather than the absolute mechanical features of the hydrogels, is essential to guide the directional cell migration. The results demonstrated that cells migrate preferentially toward hydrogel regions that mimic the viscoelastic properties of their native tissues by mechanosensing the analog viscoelastic properties of synthetic gradient hydrogel substrates, toward adhesion and migration properties.

Moreover, Fig. 2 displays the average spreading area of the three cell lines on the corresponding overlapping HAG hydrogels. The C2C12 cells exhibited a maximum averaged spreading area of 1166 μm^2 when seeded on HAG-2 muscle-mimicking hydrogel,[74] while the spreading on the other two hydrogel compositions (HAG-1, HAG-3) demonstrated no statistical significance between each other, but substantially smaller cell spreading area as compared to cells grown on HAG-2, Fig. 2A(iii). Likewise, NIH-3T3 cells seeded on HAG-3 epidermis mimetic hydrogel revealed a maximum averaged spreading area of 1164 μm^2, while the spreading on the other two hydrogel compositions (HAG-2, HAG-4) demonstrated no statistical significance between each other, but substantially smaller cell spreading area as compared to cells grown on HAG-3,[75] Fig. 2B(iii). Similarly, chondrocyte cells seeded on HAG-4 cartilage mimetic hydrogel composition revealed a maximum averaged spreading area of 941 μm^2, and a substantially smaller spreading area when grown on HAG-3 or HAG-5,[76] Fig. 2C(iii). That is, the viscoelastic properties of the hydrogel substrates control not only the migration directionality of the cells but also regulate their spreading area on different hydrogel substrates. The results suggest that the spreading and migration properties are driven by dynamic mechanical forces induced by the gradient viscoelastic properties of the hydrogel matrices.

3.4. Viscoelasticity modulated cell-traction forces on HAG hydrogels

To further characterize the mechanical forces exerted by adherent cells on the hydrogel substrates, we used the traction force microscopy (TFM) method.[77–80] This technique provides a quantitative method for evaluating the contractile forces exerted by cells, which are transmitted to the extracellular matrix (ECM) or synthetic substrates *via* focal adhesions. According to this method, fluorescent beads are embedded as markers in the viscoelastic matrix. The cells adherent to the

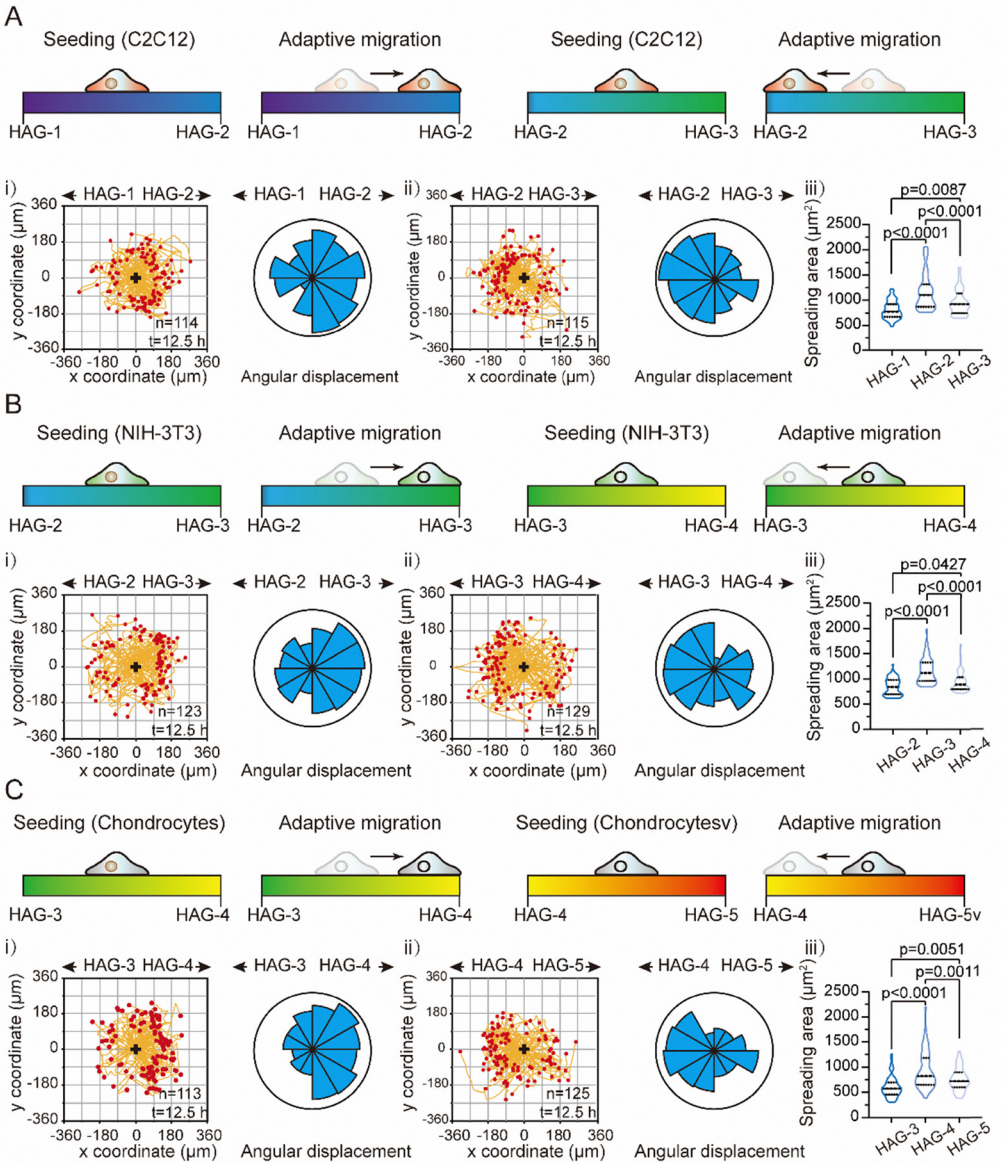

Fig. 2 Adaptive directed migration cell migration dictated by gradient hydrogel viscoelasticity and cell spreading areas of the cells and variable viscoelastic gels: (A) (i) schematic directed C2C12 cell migration positioned at different sites of a gradient hydrogel composite consisting of HAG-1, HAG-2, and HAG-3. (ii) Left – cell migration trajectories taken after 12.5 hours from seeding the cells at the central position of the interconnecting boundary between HAG-1 and HAG-2. Right – angular displacement of analyzed cell migration trajectories. (iii) Left – migration trajectories of C2C12 cells positioned at the center of HAG-2 and HAG-3 boundary. Right – angular displacement of analyzed cell migration trajectories. (iii) Spreading areas of C2C12 cells on HAG-1, HAG-2, and HAG-3, composed of constant pre-designed viscoelasticity. (B) (i) Schematic preferred cell migration of NIH-3T3 cells on HAG-2/HAG-3 or HAG-3/HAG-4 hydrogel substrate. (ii) Cell migration trajectories (and angular displacement), positioned at: left – the center of HAG-2/HAG-3, and right – at the center of HAG-3/HAG-4. (iii) spreading areas of NIH-3T3 cells on distinct preprogramed viscoelastic hydrogels HAG-2, HAG-3, and HAG-4. (C) (i) Schematic mechanosensing-induced directed migration of chondrocyte cells seeded at the intersection of HAG-4/HAG-4 or HAG-4/HAG-5. (ii) Substrate-induced cell migration trajectories (and angular displacement) of chondrocyte cells positioned at: left – center of interconnected HAG-3/HAG-4, and right – center of HAG-4/HAG-5. (iii) Spreading areas analysis of chondrocyte cells seeded on the viscoelastic HAG-3, HAG-4, and HAG-5.

viscoelastic substrate pull the matrix-embedded beads, thereby deforming their microscopic positions. By fluorescent microscopy imaging of the spatial position of fluorescent beads before cell adherence and after cell wash, the degree of displaced pattern of the bead markers is evaluated. Using elasticity theory models, the displacement patterns are converted into traction stress maps, which display quantitative stress values characterizing the mechanical forces exerted by adherent cells on the substrate. Accordingly, the three cell types, C2C12 myoblasts, NIH-3T3 fibroblasts, and mouse chondrocytes, were each cultured on the five well-defined viscoelastic bead-embedded hydrogel substrates (HAG-1–HAG-5).

The mechanical traction forces of the cells, characterizing the cells adherence on the different gel frameworks, were

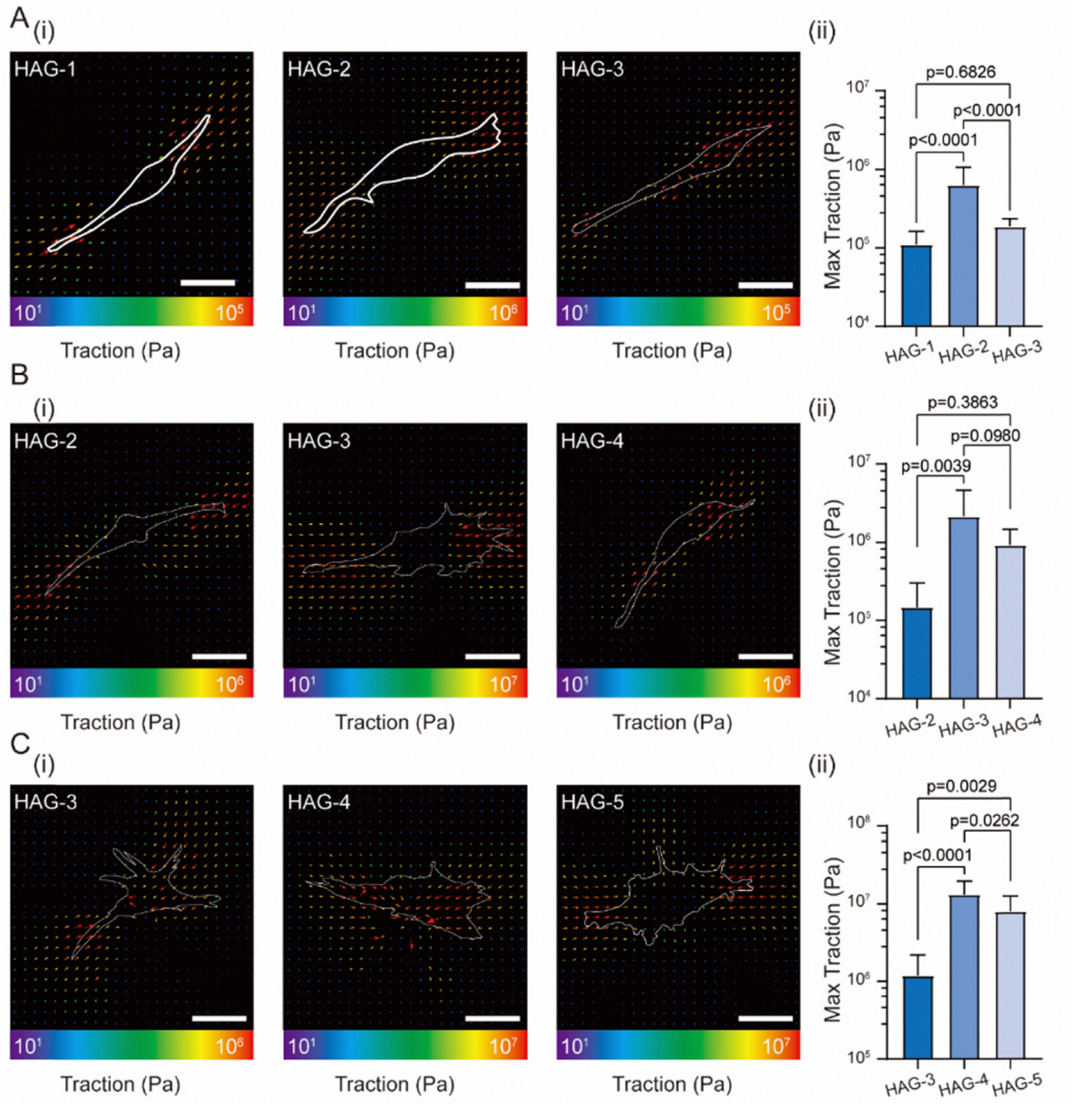

Fig. 3 Force-traction microscopy (TFM) images of fluorescent beads embedded in HAG hydrogels, subjected to displacement by mechanosensing-induced, single-cell adhesion. (A) (i) TFM image corresponding to C2C12 cells interacting with pre-programmed HAG-1, HAG-2, and HAG-3. (ii) Maximum traction force values corresponding to the interactions between C2C12 cells with the respective hydrogels (derived upon analyzing the traction stress maps reconstructed from bead-displacement vectors for each hydrogel, error bars derived from $N = 3$ experiments). (B) (i) TFM analysis of NIH-3T3 cells seeded on the respective HAG, distinct pre-programmed hydrogels HAG-2, HAG-3, and HAG-4. (ii) Max traction force values of NIH-3T3 cells on the respective HAG hydrogels. (C) (i) TFM images, and (ii) max traction force induced by chondrocyte cells on HAG-3, HAG-4, and HAG-5 hydrogels.

evaluated and exemplified in Fig. 3 and Fig. S15. The experimental C2C12 traction forces on the three gels, HAG-1, HAG-2, and HAG-3, are displayed in Fig. 3A(i). The maximum traction force of the cells evaluated from a collection of cells (C2C12 Cells), Fig. 3A(ii), is observed on the HAG-2 hydrogel (85 kPa), compared to considerably lower forces observed on the softer HAG1 (18 kPa) or higher stiffness HAG-3 (230 kPa). Therefore, the stress associated with cell traction forces exerted by the C2C12 cells with HAG-2 hydrogel correlates well with the mechanosensing preference for HAG-2 viscoelasticity, demonstrating a preferred adherence of the C2C12 cells onto HAG-2 over HAG-1 and HAG-3. Moreover, NIH-3T3 cells exerted traction forces on the three gels, HAG-2, HAG-3, and HAG-4, as displayed in Fig. 3B(i). The maximum traction force of the cells evaluated from NIH-3T3 cells, Fig. 3B(ii), is observed on the HAG-3 hydrogel (230 kPa), as compared to considerably lower forces observed on the softer HAG-2 (18 kPa) or higher stiffness HAG-4 (230 kPa). That is, the stress associated with cell traction forces exerted by the NIH-3T3 cells with HAG-3 hydrogel correlates well with the mechanosensing preference for HAG-3 viscoelasticity, demonstrating a preferred adherence of the NIH-3T3 cells onto HAG-3 over HAG-2 and HAG-4. Similarly, the force exerted by the chondrocytes on HAG-3, HAG-4, and HAG-5 is displayed in Fig. 3C(i). The maximum traction force of the cells evaluated from chondrocytes, Fig. 3C(ii), is observed on the HAG-4 hydrogel (654 kPa), while revealing significantly

lower forces on the softer HAG-3 (18 kPa) and lower forces on the higher stiffness HAG-5 (230 kPa), demonstrating preferred adherence on HAG-4 viscoelasticity as compared to HAG-3 and HAG-5. Collectively, all three cell types demonstrate enhanced forces exerted to the surface of the viscoelastic hydrogel, displaying similar properties mimicking their native tissue.

The quantitative mechano-adherent features of the cells with the hydrogel matrices reflect the mechanosensing interactions of the cells with the substrate viscoelasticity. The traction force microscopy results fit well with the mechanosensing features of the viscoelastic substrate. It is worth noting that the traction force microscopy results correlate well with the cell spreading area results. That is, the cells demonstrated a preference for spreading and cell adherence upon cultivation on regions that resemble their native tissue's viscoelasticity over hydrogels differing in their viscoelastic properties. Moreover, as asymmetric traction forces drive cell polarization and migration towards areas of higher forces, these findings likely explain the observed viscoelasticity-directed cell migration on these gradient hydrogels.

3.5. Hydrogel viscoelasticity-dictated cellular focal adhesion maturation

The studies described in Sections 3.1–3.4 present biomimetic modeling of cell-ECM interactions by probing mechanosensing and mechano-force interactions between different cell lines and synthetic hydrogels exhibiting varying viscoelasticity, by analyzing single cells within a colony environment. The study introduced controlled directional migration on gradient hydrogels, as well as traction force microscopy measurements on different viscoelastic hydrogels, demonstrating a tight relationship between the native tissue mechanoproperties (Y modulus and $\tau_{1/2}$) and the viscoelastic parameters of the synthetic hydrogel substrates.

The migration/adhesion features in nature involve, however, complex biochemical cues controlled by cell–extracellular matrix (ECM) interactions leading to the formation or dissociation of focal adhesion (FA) complexes, which regulate intracellular cytoskeleton activity toward the assembly of FA protein complexes and their maturation. These include the mechano-responsive actin-induced phosphorylation/dephosphorylation of the YAP/TAZ proteins, which, upon dephosphorylation, are translocated into the cell nuclei, acting as transcriptional co-activators expressing FA maturation protein complexes.[13,77,78,81] That is, favored cell-ECM interactions mediate actin-based signaling, enhancing FA maturation. In contrast, disfavored cell–ECM interactions are anticipated to weaken actin-based signaling toward FA maturation. Accordingly, we argued that the quantitative evaluation of the YAP/TAZ distribution ratio between the cytoplasm and the nuclei across different cell lines, as a function of the viscoelastic properties of the hydrogel substrates, could provide molecular insights into the transformation of mechanosensing functions to respective intracellular responses. Moreover, the phosphorylation/dephosphorylation of YAP/TAZ is influenced by various converging signals beyond FA, including GPCR signaling, energy stress, and others, resulting in changes in p-YAP concentration dominated by different factors.[82–84] Thus, identification of additional parameters reflecting the YAP/TAZ translocation ratio is important. These include, for example, the quantitative evaluation of phosphorylated focal adhesion kinase (p-FAK), reflecting the phosphorylation site of focal adhesion kinase (FAK),[85,86] or of vinculin, a distinct protein that stabilizes FA complexes, which was reported as an efficient biomarker assaying the FA maturation.[87–89] Thus, in the following section, we adapt the quantitative evaluation of different cellular probes and markers to probe, at the molecular level, the relationship between mechanosensing cell properties and the viscoelastic properties of the hydrogel substrate environments.

Indeed, immunoblotting assays corresponding to vinculin and p-FAK demonstrated elevated levels of vinculin and p-FAK in C2C12, NIH-3T3, and chondrocyte cells upon culturing on hydrogels matching their respective tissue viscoelasticity (HAG-2, HAG-3, and HAG-4), Fig. 4A and B. That is, C2C12 cells demonstrated enhanced FA maturation on the HAG-2 hydrogel, as compared to HAG-3 and HAG-4, whereas NIH-3T3 cells demonstrated preferred FA maturation on HAG-3, as compared to HAG-2 and HAG-4, and the chondrocyte cells revealed enhanced FA maturation on HAG-4, as compared to HAG-3 and HAG-5. In addition, immunofluorescence assays imaging the mean fluorescence intensity (MFI) of p-FAK associated with FA formation and maturation of C2C12 cells on the corresponding hydrogel substrates (HAG-1 to HAG-5) are displayed in Fig. 4D and F(ii), demonstrating enhanced MFI of p-FAK formation on HAG-2, as compared to HAG-1, HAG-3, HAG-4, and HAG-5. Also, Fig. 4E and F(iii) depict the sizes of the FA complexes of C2C12 cells on the different hydrogels, demonstrating enhanced dimensions of FA on the hydrogel exhibiting viscoelasticity properties matching their native tissue (HAG-2). Moreover, the localization of the transcriptional regulator YAP, associated with the culturing of C2C12 cells on the respective hydrogels, was assayed by immunofluorescence imaging, Fig. 4C and F(i). Evidently, the YAP associated with C2C12 cells cultured on the HAG-2 hydrogel revealed significantly increased nuclear localization, as compared to C2C12 cells cultured on HAG-1, HAG-3, HAG-4, or HAG-5. These results are consistent with the favored mechanosensing properties of C2C12 cells cultured on the HAG-2, demonstrating the link between the localization of transcriptional regulator YAP and the viscoelastic matching properties between the hydrogel/cells. Similar results were also presented for NIH-3T3 cells and chondrocytes, with favored mechanosensing performances in corresponding viscoelastic hydrogels (Fig. S16 and S17). To further validate that this mechanosensing-induced nuclear translocation translates into functional transcriptional activity, we evaluated the mRNA expression of connective tissue growth factor (CTGF), a primary downstream target gene of the YAP/TAZ pathway. As shown in Fig. S18, quantitative PCR (qPCR) analysis revealed that CTGF expression was significantly upregulated in cells cultured on hydrogels matching their native tissue viscoelasticity. Specifically, C2C12 cells exhibited the highest CTGF expression on HAG-2, whereas NIH-3T3 and chondrocyte cells demonstrated peak-expression levels on HAG-3 and HAG-4, respectively. This robust downstream transcriptional activity is highly consistent with the

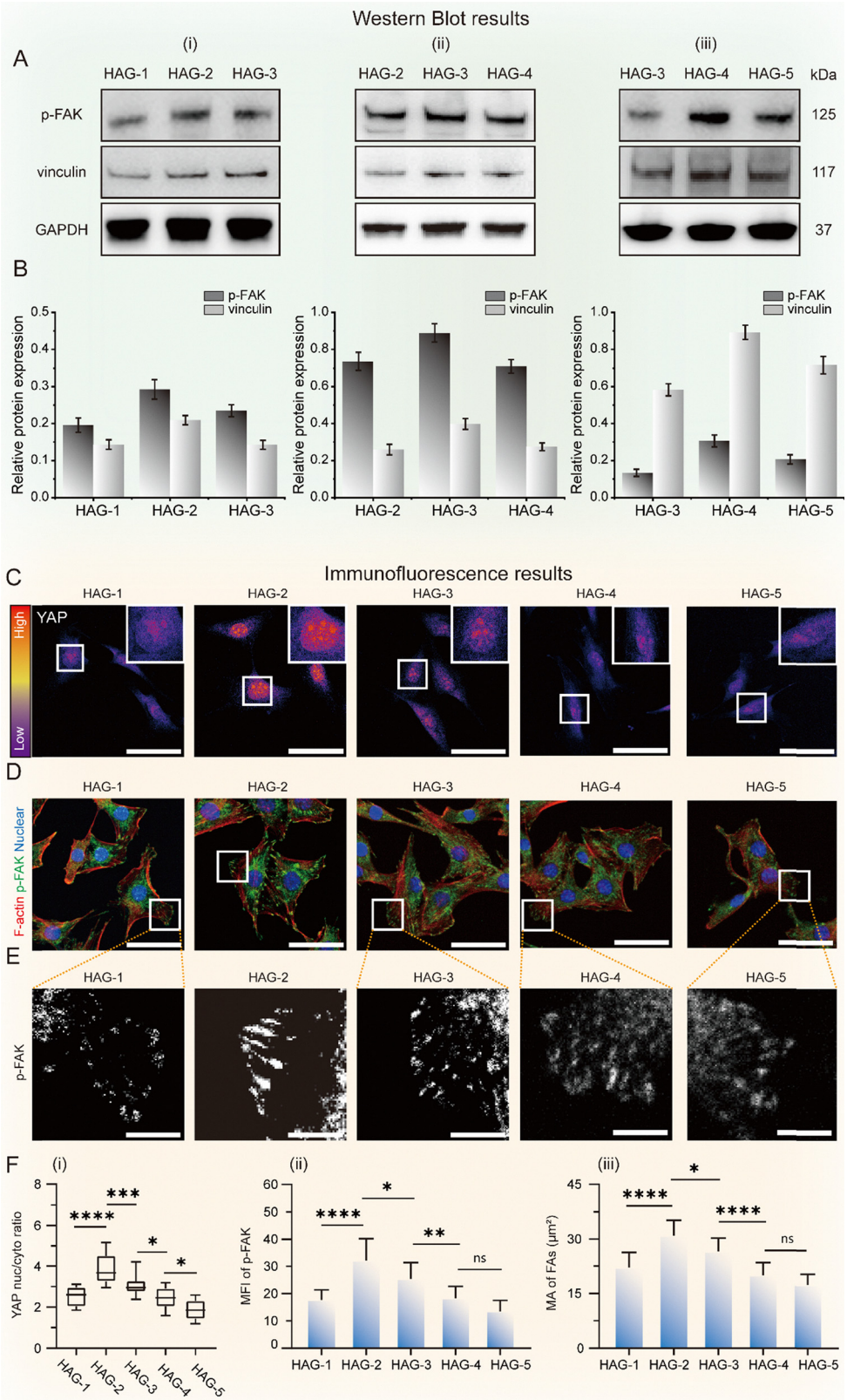

Fig. 4 (A) Analysis of the adaptive mechanosensing cell-viscoelastic hydrogels interactions on the focal adhesion (FA) maturation process by probing the intracellular levels of p-FAK/vinculin levels using Western blots corresponding to p-FAK and vinculin, generated in: (i) C2C12 cells seeded on preprogrammed distinct HAG-1, HAG-2, and HAG-3 hydrogels, (ii) NIH-3T3 cells seeded on the viscoelastic HAG-2, HAG-3, and HAG-4 hydrogel substrates, and (iii) chondrocyte cells seeded on HAG-3, HAG-4, and HAG-5 hydrogel substrates. In all experiments, GAPDH was probed as a control. (B) Quantitative analysis of the content of the expressed p-FAK and vinculin levels corresponding to the experiment displayed in (A), total $N = 3$ experiments for each HAG-1/HAG-2/HAG-3; HAG-2/HAG-3/HAG-4; HAG-3/HAG-4/HAG-5 systems. (C) Imaging the immunoassayed YAP biomarker in the nucleus

and cytoskeletal regions of C2C12 cells interacting with pre-programmed viscoelastic HAG-1, HAG-2, HAG-3, HAG-4, and HAG-5 hydrogel substrates. (D) Confocal microscopy images corresponding to immunoassayed p-FAK biomarker in C2C12 cells interacting with the different HAG gel substrates. (E) Imaging the FA sites associated with C2C12 cells interacting with different HAG hydrogels and their maturation. (F) (i) YAP nuclei/cytosol ratio corresponding to C2C12 cells interacting with different HAG hydrogel substrates. (ii) Mean fluorescent intensity (MFI) of p-FAK in C2C12 cells mechanosensing different HAG hydrogels exhibiting programmed viscoelasticity. (iii) Mean areas of FA sites associated with C2C12 cells interacting with the different HAG hydrogels. For images of p-FAK, YAP translocation ratio, MFI, and mean FA areas of different cell lines interacting with the HAG hydrogel substrates, see Fig. S15–17.

YAP nuclear localization profiles, confirming that the substrate-dictated mechanosensing signals are successfully transduced into downstream gene regulation. Altogether, these results indicate that substrate viscoelasticity, particularly when matching native physiological values, has a strong influence on YAP/TAZ pathway activation, focal adhesion formation and maturation, and directed migration.

3.6. Spatial separation of cells by programmable viscoelastic substrates

The study introduced the fundamental perspective landscape relating the mechanosensing properties of cells to the programmable viscoelasticity of gradient hydrogel substrate on the cell spreading area, FA maturation, and directional migration. We searched, however, for a potential application of these basic phenomena. In the next section, we address the possible spatial separation of a mixture of two different cell types by viscoelasticity-tailored substrates. To distinguish the different cell types, NIH-3T3 cells were transfected to express GFP, C2C12 cells to express mCherry, and chondrocytes remained unlabeled. Fig. 5 presents experiments separating different mixtures of cells by a gradient gel substrate consisting of three ordered gradient hydrogel combinations composed of HAG-2, HAG-3, and HAG-4. In the first experiment, a mixture of C2C12 and NIH-3T3 cells was randomly seeded on a hydrogel composed of HAG-2/HAG-3 gradient gel domains. Accordingly, the migration of the seeded cell mixture on the gradient hydrogel substrate is anticipated to lead to mechanosensing-induced separation of the cells, resulting in the separation of C2C12 cells toward the HAG-2 domain and of NIH-3T3 cells toward the HAG-3 domain. This is attributed to the adaptive migration and adhesion features of the cells on the respective substrates, dictated by the matching between the mechanical properties of the tissues, and the substrate viscoelasticity, as schematically presented in Fig. 5A(i). The experimental confocal microscopy images, and the quantitative analysis of cell distribution on the HAG-2/HAG-3 substrate, immediately after seeding and after a time interval of 3 days, are depicted in Fig. 5A(ii). Clearly, after this time interval, the two cell types are spatially separated. While the C2C12 cells are centralized on the HAG-2 domain, the NIH-3T3 cells are localized on the HAG-3 domain. Quantitative analysis of the cell distribution after 3 days demonstrate successful separation, with sorting purities of 77.33% for C2C12 onto HAG-2 and 58.44% for NIH-3T3 onto HAG-3. The corresponding separation efficiencies are 64.44% and 72.58%, respectively (Table S4).

Similarly, Fig. 5B depicts the substrate-induced separation of a mixture consisting of the NIH-3T3 and chondrocyte cells. In this case, the cell mixture was randomly seeded on a HAG-3/HAG-4 gradient hydrogel substrate. While the NIH-3T3 mechanosensing features match the HAG-3 region, the chondrocyte cells match the HAG-4 viscoelastic properties. Accordingly, the substrate-induced separation of the cells is anticipated to follow the pattern shown schematically in Fig. 5B(i). The experimental confocal microscopy images and quantitative analysis of the mechanosensing viscoelasticity-dictated, separation of the cells are displayed in Fig. 5B(ii) and Table S4. After 3 days, the chondrocytes on the HAG-4 domain reached a sorting purity of 60.20%, while the NIH-3T3 cells on the HAG-3 domain exhibited a higher purity of 77.94%. The separation efficiencies for chondrocytes and NIH-3T3 cells were 79.73% and 57.61%, respectively. The results confirm that after a time interval of 3 days, the two types of cells are separated, according to the mechanosensing-guided adaptation of the matching parameters between the tissue cells viscoelasticity and the respective hydrogel regions. Moreover, Fig. 5C presents the separation of a mixture containing C2C12 and chondrocyte cells seeded on HAG-2/HAG-4 gradient substrate that includes viscoelasticity of the two cell types, Fig. 5C(i). Effective separation of the cell mixture is observed, Fig. 5C(ii) and Table S4. The sorting purity reached 76.92% for C2C12 on HAG-2 and 82.28% for chondrocytes on HAG-4. The separation efficiency was also high for both cell types, recorded at 78.13% for C2C12 and 81.25% for chondrocytes, validating the robust control of cell localization *via* mechanosensing, matching with specific viscoelastic regions.

4. Conclusions

The study introduced a versatile method for synthesizing hydrogel matrices exhibiting programmable viscoelasticity. The method enables precise control over the hydrogels compositions and demonstrates reproducibility and scalability. The synthetic viscoelastic programmable hydrogel substrates mimic native extracellular matrix (ECM) functions, regulating mechanical cell sensing and responses. Native ECM properties regulating mechanical cell functions, such as adhesion and migration, resulting in mechanosensing and focal adhesion maturation, were mirrored by synthetic hydrogels, exhibiting programmable and gradient viscoelasticity. The study demonstrated the relationships between mechanosensing interactions of different cell types and hydrogel frameworks of variable and gradient viscoelasticities, and their responsive signaling or intracellular cues controlling cytoskeleton pathways. These were reflected by the translation of mechanosensing interactions between the cells and the synthetically programmable viscoelastic hydrogels into mechanical cell functions, such as cell spreading, focal adhesion

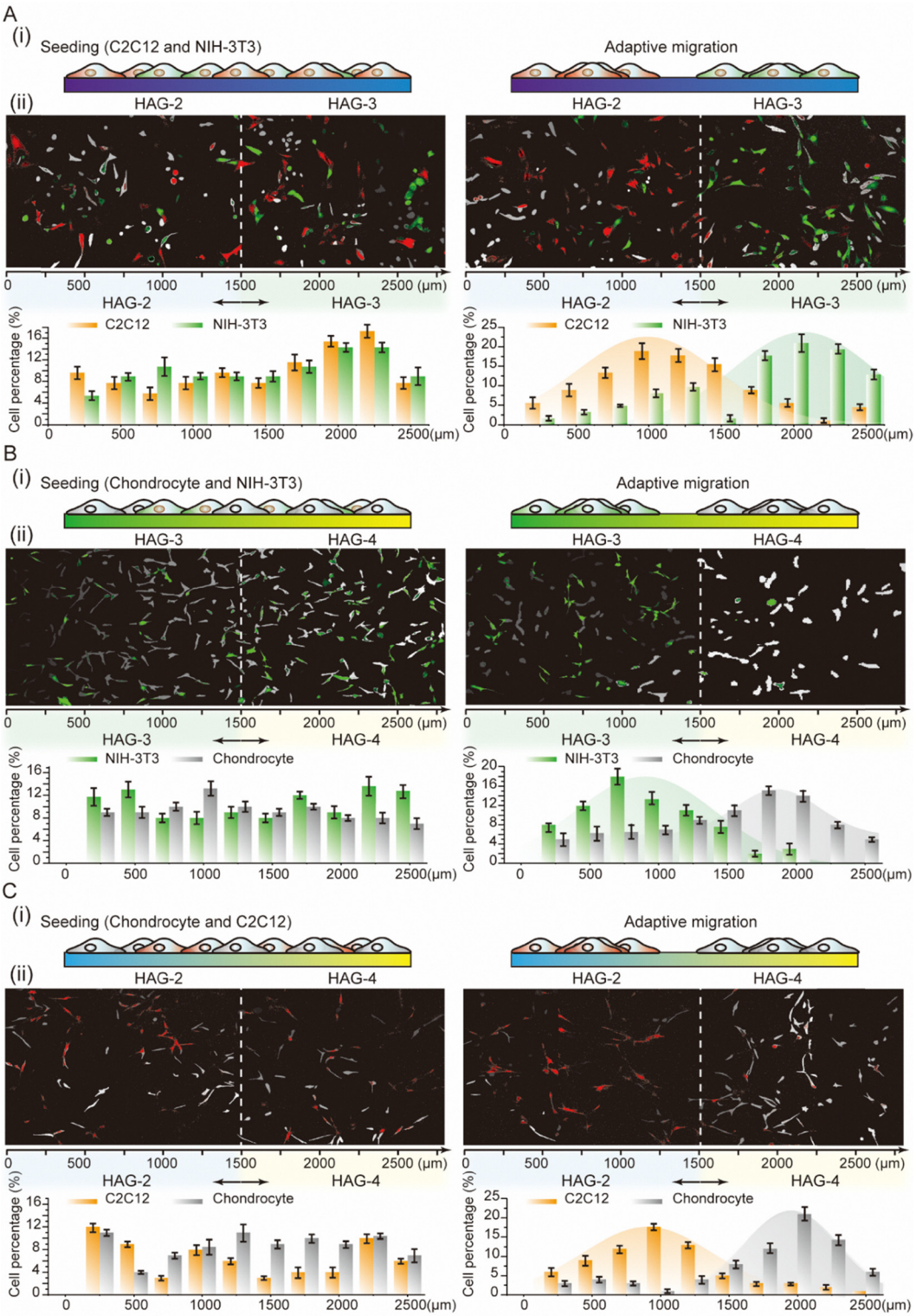

Fig. 5 Mechanosensing-induced separation of different cell mixtures by the application of two interlinked viscoelastic gradient HAG gels upon seeding the mixture randomly on the gel substrates and probing spatial cell distribution after 3 days of viscoelastic-dictated migration of the cells. (A) (i) Schematic seeding and separation of C2C12/NIH-3T3 cells mixture on a HAG-2/HAG-3 gradient gel substrate. (ii) Confocal microscopy images of left- immediately after randomly seeding the cell mixture, C2C12 (red) and NIH-3T3 (green), right – after 3 days of cell separation. Bottom – positional relative cell count, after seeding (left), and after separation. (B) (i) schematic separation of NIH-3T3 and chondrocyte (grey) cells mixture from randomly distributed cells (left) on gradient viscoelastic gel substrate composed of HAG-3/HAG-4, to the mechanosensing-induced directional migration of the cells to their matching viscoelastic hydrogel domain. (ii) Confocal images corresponding to left – the randomly distributed seeded cells, right – separated cells after 3 days. Bottom – relative cell counting according to their position. (C) (i) Schematic separation of C2C12/chondrocyte cell mixture seeded on the gradient joint gel substrates composed of HAG-2/HAG-4. (ii) Confocal images corresponding to the randomly distributed cell mixture (left), and of the separated cell after 3 days (right). Bottom – positional relative cell counting corresponding to the randomly distributed cells and the separated cells.

maturation, and dictated spatiotemporal migration. The control of mechanical cell functions *via* mechanosensing of the viscoelasticities of hydrogel matrices was successfully applied for the hydrogel-guided dynamic separation of different mixtures of cells.

The practical utility and future applications of the research results are indispensable. By spatiotemporal mechanical movement of the substrate on which the hydrogel is deposited, patterns of complex hydrogel frameworks of different preprogrammed viscoelasticity properties may be generated. Such hydrogel arrays would allow autonomous programmed patterning of cells and their functional intercommunication. Furthermore, the design of cell-programmable viscoelastic hydrogel arrays for controlled differentiation of stem cells or cancer research could provide effective synthetic substrates for high-throughput synthesis of target cells for tissue engineering, immunotherapy, and regenerative medicine. Moreover, the results demonstrating the "dialog" between different cells and the viscoelasticity of hydrogels on the mechanosensing and subsequent mechanical cell functions can be extended to new directions, probing cell interactions with synthetic viscoelastic hydrogel interfaces. Chemical modification of cell membranes with chemical agents is anticipated to control cell behavior on viscoelastic hydrogel substrates. Similarly, integration of stimuli-responsive elements into the hydrogel matrices[90] would allow the triggered control of the viscoelasticity of the substrates, thereby enabling the switchable[91–93] or transient[94] mechanosensing and accompanying mechanical properties of the cells. Moreover, the fabrication of cryogels[95] and gradient cryogels,[96–98] and the identification of the functional features of cryostructures within the resulting cell-viscoelastic composition and mechanosensing properties could introduce new dimensions to the systems. Also, comprehensive experimental and theoretical biophysical characterization of the links between mechanosensing interactions of synthetic viscoelastic hydrogels and intracellular signaling cues could be an interesting path to follow.

Author contributions

Z. L., Y. G., I. W., and J. Z. designed the research; Z. L. and J. Z. designed the hydrogel engineering approach; H. Y., M. L., Y. M., and Y. S. synthesized the hydrogel; H. Y., M. L., and L. C. performed all biological experiments; Z. L., H. Y., Y. G., G. D. R., and J. Z. analyzed data; Z. L., Y. G., J. Z., G. D. R., and I. W. wrote the paper.

Conflicts of interest

There is no conflict of interest to report.

Data availability

The data supporting this article are included in the SI. Supplementary information available: Tables S1–S3, Fig. S1–S16, and further experimental details. Oxidation degree characterization of oxi-HA, FTIR spectroscopy, SEM imaging, rheological and nanoindentation measurements, and cell viability of HAG hydrogels. See DOI: https://doi.org/10.1039/d6tb00438e.

Acknowledgements

This work is supported by the National Key R&D Program of China (2023YFF0722600), NSFC (22122803, 22378121, 22105070, 32350018), Science and Technology Commission of Shanghai Municipality (24DX1400200), and the Fundamental Research Funds for the Central Universities (222201717003). JZ acknowledges Shanghai Natural Science Foundation Project (23ZR1479500, 23JC1401700). ZL acknowledges Shanghai Sailing Program (20YF1410300).

References

1 J. D. Humphrey, E. R. Dufresne and M. A. Schwartz, Mechanotransduction and extracellular matrix homeostasis, *Nat. Rev. Mol. Cell Biol.*, 2014, **15**(12), 802–812.
2 A. W. Holle, J. L. Young, K. J. Van Vliet, R. D. Kamm, D. Discher, P. Janmey, J. P. Spatz and T. Saif, Cell-extracellular matrix mechanobiology: forceful tools and emerging needs for basic and translational research, *Nano Lett.*, 2018, **18**(1), 1–8.
3 X. Di, X. Gao, L. Peng, J. Ai, X. Jin, S. Qi, H. Li, K. Wang and D. Luo, Cellular mechanotransduction in health and diseases: from molecular mechanism to therapeutic targets, *Signal Transduct. Target. Ther.*, 2023, **8**(1), 282.
4 A. Saraswathibhatla, D. Indana and O. Chaudhuri, Cell-extracellular matrix mechanotransduction in 3D, *Nat. Rev. Mol. Cell Biol.*, 2023, **24**(7), 495–516.
5 P. Lappalainen, T. Kotila, A. Jégou and G. Romet-Lemonne, Biochemical and mechanical regulation of actin dynamics, *Nat. Rev. Mol. Cell Biol.*, 2022, **23**(12), 836–852.
6 P. Kanchanawong and D. A. Calderwood, Organization, dynamics and mechanoregulation of integrin-mediated cell-ECM adhesions, *Nat. Rev. Mol. Cell Biol.*, 2023, **24**(2), 142–161.
7 K. Katoh, Integrin and its associated proteins as a mediator for mechano-signal transduction, *Biomolecules*, 2025, **15**(2), 166.
8 T. D. Pollard and J. A. Cooper, Actin, a central player in cell shape and movement, *Science*, 2009, **326**(5957), 1208–1212.
9 J. Mishra, S. Chakraborty, N. Mahto, A. Roy, S. Manna, T. Baral, P. Nandi and S. K. Patra, Mechanotransduction and epigenetic modulations of chromatin: role of mechanical signals in gene regulation, *J. Cell. Biochem.*, 2024, **125**(3), e30531.
10 R. Cao, H. Tian, Y. Tian and X. Fu, A hierarchical mechanotransduction system: from macro to micro, *Adv. Sci.*, 2024, **11**(11), e2302327.
11 F. Martino, A. R. Perestrelo, V. Vinarský, S. Pagliari and G. Forte, Cellular mechanotransduction: from tension to function, *Front. Physiol.*, 2018, **9**, 824.
12 H. Jafarinia, A. Khalilimeybodi, J. Barrasa-Fano, S. I. Fraley, P. Rangamani and A. Carlier, Insights gained from

computational modeling of YAP/TAZ signaling for cellular mechanotransduction, *NPJ Syst. Biol. Appl.*, 2024, **10**(1), 90.
13 X. Cai, K.-C. Wang and Z. Meng, Mechanoregulation of YAP and TAZ in cellular homeostasis and disease progression, *Front. Cell Dev. Biol.*, 2021, **9**, 673599.
14 K. E. Scott, S. I. Fraley and P. Rangamani, A spatial model of YAP/TAZ signaling reveals how stiffness, dimensionality, and shape contribute to emergent outcomes, *Proc. Natl. Acad. Sci. U. S. A.*, 2021, **118**(20), e2021571118.
15 W. H. Goldmann, Mechanotransduction and focal adhesions, *Cell Biol. Int.*, 2012, **36**(7), 649–652.
16 T. Shemesh, B. Geiger, A. D. Bershadsky and M. M. Kozlov, Focal adhesions as mechanosensors: a physical mechanism, *Proc. Natl. Acad. Sci. U. S. A.*, 2005, **102**(35), 12383–12388.
17 S. J. Tan, A. C. Chang, S. M. Anderson, C. M. Miller, L. S. Prahl, D. J. Odde and A. R. Dunn, Regulation and dynamics of force transmission at individual cell-matrix adhesion bonds, *Sci. Adv.*, 2020, **6**(20), eaax0317.
18 J. Kim, A possible molecular mechanism for mechanotransduction at cellular focal adhesion complexes, *Biophys. Rep.*, 2021, **1**(1), 100006.
19 A. E. Miller, P. Hu and T. H. Barker, Feeling things out: bidirectional signaling of the cell–ECM interface, implications in the mechanobiology of cell spreading, migration, proliferation, and differentiation, *Adv. Healthc. Mater.*, 2020, **9**(8), e1901445.
20 R. J. Leiphart, D. Chen, A. P. Peredo, A. E. Loneker and P. A. Janmey, Mechanosensing at cellular interfaces, *Langmuir*, 2019, **35**(23), 7509–7519.
21 N. C. Gauthier and P. Roca-Cusachs, Mechanosensing at integrin-mediated cell–matrix adhesions: from molecular to integrated mechanisms, *Curr. Opin. Cell Biol.*, 2018, **50**, 20–26.
22 A. Martinet, L. Miebach, K.-D. Weltmann, S. Emmert and S. Bekeschus, Biomimetic hydrogels – tools for regenerative medicine, oncology, and understanding medical gas plasma therapy, *Small*, 2025, **21**(9), e2403856.
23 F. J. Vernerey, S. Lalitha Sridhar, A. Muralidharan and S. J. Bryant, Mechanics of 3D cell–hydrogel interactions: experiments, models, and mechanisms, *Chem. Rev.*, 2021, **121**(18), 11085–11148.
24 M. E. Allen, J. W. Hindley, N. O'Toole, H. S. Cooke, C. Contini, R. V. Law, O. Ces and Y. Elani, Biomimetic behaviors in hydrogel artificial cells through embedded organelles, *Proc. Natl. Acad. Sci. U. S. A.*, 2023, **120**(35), e2307772120.
25 L. Rijns, M. B. Baker and P. Y. W. Dankers, Using chemistry to recreate the complexity of the extracellular matrix: guidelines for supramolecular hydrogel–cell interactions, *J. Am. Chem. Soc.*, 2024, **146**(26), 17539–17558.
26 B. G. Soliman, A. K. Nguyen, J. J. Gooding and K. A. Kilian, Advancing synthetic hydrogels through nature-inspired materials chemistry, *Adv. Mater.*, 2024, **36**(42), e2404235.
27 A. F. Roca-Arroyo, J. A. Gutierrez-Rivera, L. D. Morton and D. A. Castilla-Casadiego, Hydrogel network architecture design space: impact on mechanical and viscoelastic properties, *Gels*, 2025, **11**(8), 588.
28 R. S. Stowers, S. C. Allen and L. J. Suggs, Dynamic phototuning of 3D hydrogel stiffness, *Proc. Natl. Acad. Sci. U. S. A.*, 2015, **112**(7), 1953–1958.
29 N. R. Richbourg, M. Wancura, A. E. Gilchrist, S. Toubbeh, B. A. C. Harley, E. Cosgriff-Hernandez and N. A. Peppas, Precise control of synthetic hydrogel network structure *via* linear, independent synthesis-swelling relationships, *Sci. Adv.*, 2021, **7**(7), eabe3245.
30 C. Wang and J. Zhang, Recent advances in stimuli-responsive DNA-based hydrogels, *ACS Appl. Bio Mater*, 2022, **5**(5), 1934–1953.
31 D. E. Discher, P. Janmey and Y.-L. Wang, Tissue cells feel and respond to the stiffness of their substrate, *Science*, 2005, **310**(5751), 1139–1143.
32 C. Zhang, Y. Tan, J. Feng, C. Huang, B. Liu, Z. Fan, B. Xu and T. Lu, Exploration of the effects of substrate stiffness on biological responses of neural cells and their mechanisms, *ACS Omega*, 2020, **5**(48), 31115–31125.
33 J. Lou and D. J. Mooney, Chemical strategies to engineer hydrogels for cell culture, *Nat. Rev. Chem.*, 2022, **6**(10), 726–744.
34 F. Milos and A. del Campo, Polyacrylamide hydrogels as versatile biomimetic platforms to study cell–materials interactions, *Adv. Mater. Interfaces*, 2024, **11**(34), 2400404.
35 A. D. Rape, M. Zibinsky, N. Murthy and S. Kumar, A synthetic hydrogel for the high-throughput study of cell–ECM interactions, *Nat. Commun.*, 2015, **6**(1), 8129.
36 B. Trappmann, J. E. Gautrot, J. T. Connelly, D. G. T. Strange, Y. Li, M. L. Oyen, M. A. Cohen Stuart, H. Boehm, B. Li, V. Vogel, J. P. Spatz, F. M. Watt and W. T. S. Huck, Extracellular-matrix tethering regulates stem-cell fate, *Nat. Mater.*, 2012, **11**(7), 642–649.
37 T. A. Al-Hilal, M.-A. Chrysovergi, P. E. Grasberger, F. Liu, V. Auernheimer, Y. Zhou, Z. Xiao, M. A. Leon-Duque, A. Santos, T. Islam, M. Ligorio, D. Sicard, C. K. Probst, V. Vrbanac, T. S. Reddi, L. Vincent, C. Happe, E. Chaum, C. R. Yates, K. Daneshvar, A. C. Mullen, D. Ting, E. S. White, R. Kalluri, C. M. Woo, E. Puré, W. H. Goldmann, J. L. Alonso, A. M. Tager, A. J. Engler, D. J. Tschumperlin and D. Lagares, Durotaxis is a driver and potential therapeutic target in lung fibrosis and metastatic pancreatic cancer, *Nat. Cell Biol.*, 2025, **27**(9), 1543–1554.
38 C. D. Hartman, B. C. Isenberg, S. G. Chua and J. Y. Wong, Vascular smooth muscle cell durotaxis depends on extracellular matrix composition, *Proc. Natl. Acad. Sci. U. S. A.*, 2016, **113**(40), 11190–11195.
39 W. J. Hadden, J. L. Young, A. W. Holle, M. L. McFetridge, D. Y. Kim, P. Wijesinghe, H. Taylor-Weiner, J. H. Wen, A. R. Lee, K. Bieback, B.-N. Vo, D. D. Sampson, B. F. Kennedy, J. P. Spatz, A. J. Engler and Y. S. Choi, Stem cell migration and mechanotransduction on linear stiffness gradient hydrogels, *Proc. Natl. Acad. Sci. U. S. A.*, 2017, **114**(22), 5647–5652.
40 R. M. Hakeem, B. C. Subramanian, M. A. Hockenberry, Z. T. King, M. T. Butler, W. R. Legant and J. E. Bear, A photopolymerized hydrogel system with dual stiffness gradients reveals distinct actomyosin-based mechano-responses in fibroblast durotaxis, *ACS Nano*, 2023, **17**(1), 197–211.

41 K. H. Palmquist, S. F. Tiemann, F. L. Ezzeddine, S. Yang, C. R. Pfeifer, A. Erzberger, A. R. Rodrigues and A. E. Shyer, Reciprocal cell-ECM dynamics generate supracellular fluidity underlying spontaneous follicle patterning, *Cell*, 2022, **185**(11), 1960–1973.
42 V. Z. Beachley, M. T. Wolf, K. Sadtler, S. S. Manda, H. Jacobs, M. R. Blatchley, J. S. Bader, A. Pandey, D. Pardoll and J. H. Elisseeff, Tissue matrix arrays for high-throughput screening and systems analysis of cell function, *Nat. Methods*, 2015, **12**(12), 1197–1204.
43 J. P. K. Armstrong, E. Pchelintseva, S. Treumuth, C. Campanella, C. Meinert, T. J. Klein, D. W. Hutmacher, B. W. Drinkwater and M. M. Stevens, Tissue engineering cartilage with deep zone cytoarchitecture by high-resolution acoustic cell patterning, *Adv. Healthcare Mater.*, 2022, **11**(24), e2200481.
44 H. Park, T. V. Patil, S. D. Dutta, J. Lee, K. Ganguly, A. Randhawa, H. Kim and K.-T. Lim, Extracellular matrix-bioinspired anisotropic topographical cues of electrospun nanofibers: a strategy of wound healing through macrophage polarization, *Adv. Healthcare Mater.*, 2024, **13**(12), e2304114.
45 W. Liu, R. Gao, C. Yang, Z. Feng, W. Ou-Yang, X. Pan, P. Huang, C. Zhang, D. Kong and W. Wang, ECM-mimetic immunomodulatory hydrogel for methicillin-resistant *Staphylococcus aureus*-infected chronic skin wound healing, *Sci. Adv.*, 2022, **8**(27), eabn7006.
46 H. T. Ong, M. Sriram, H. H. Susapto, Y. Li, Y. Jiang, N. H. Voelcker, J. L. Young, A. W. Holle and R. Elnathan, The rise of mechanobiology for advanced cell engineering and manufacturing, *Adv. Mater.*, 2025, **37**(37), e2501640.
47 B. D. Cardoso, E. M. S. Castanheira, S. Lanceros-Méndez and V. F. Cardoso, Recent advances on cell culture platforms for *in vitro* drug screening and cell therapies: from conventional to microfluidic strategies, *Adv. Healthcare Mater.*, 2023, **12**(18), e2202936.
48 R. H. Heisser, M. Bawa, J. Shah, A. Bu and R. Raman, Soft biological actuators for meter-scale homeostatic biohybrid robots, *Chem. Rev.*, 2025, **125**(7), 3976–4007.
49 G. Cedillo-Servin, E. A. A. Al-Jehani, T. Rossy, S. P. B. Teixeira, F. Sage, R. M. A. Domingues, R. Raman and M. Castilho, Meta-adaptive biomaterials: multiscale, spatiotemporal organization and actuation in engineered tissues, *Trends Biotechnol.*, 2025, **43**(11), 2709–2723.
50 T. Morita, M. Nie and S. Takeuchi, Tetanus-driven biohybrid multijoint robots powered by muscle rings with enhanced contractile force, *Sci. Adv.*, 2025, **11**(29), eadu9962.
51 S. Mangani, M. Vetoulas, K. Mineschou, K. Spanopoulos, M. d M. Vivanco, Z. Piperigkou and N. K. Karamanos, Design and applications of extracellular matrix scaffolds in tissue engineering and regeneration, *Cells*, 2025, **14**(14), 1076.
52 J. Gao, X. Yu, X. Wang, Y. He and J. Ding, Biomaterial-related cell microenvironment in tissue engineering and regenerative medicine, *Engineering*, 2022, **13**, 31–45.
53 L. Li, S. Wang, Y. Chen, S. Dong, C. Zhang, L. Liao and W. Zhang, Hydrogels mimicking the viscoelasticity of extracellular matrix for regenerative medicine: design, application, and molecular mechanism, *Chem. Eng. J.*, 2024, **498**(155206), 155206.
54 B. Slater, J. Li, D. Indana, Y. Xie, O. Chaudhuri and T. Kim, Transient mechanical interactions between cells and viscoelastic extracellular matrix, *Soft Matter*, 2021, **17**(45), 10274–10285.
55 O. Courbot and A. Elosegui-Artola, The role of extracellular matrix viscoelasticity in development and disease, *NPJ Biol. Phys. Mech.*, 2025, **2**(1), 10.
56 Z. Liu, S. D. Ling, K. Liang, Y. Chen, Y. Niu, L. Sun, J. Li and Y. Du, Viscoelasticity of ECM and cells-origin, measurement and correlation, *Mechanobiol. Med.*, 2024, **2**(4), 100082.
57 A. Gandin, Y. Murugesan, V. Torresan, L. Ulliana, A. Citron, P. Contessotto, G. Battilana, T. Panciera, M. Ventre, A. P. Netti, L. Nicola, S. Piccolo and G. Brusatin, Simple yet effective methods to probe hydrogel stiffness for mechanobiology, *Sci. Rep.*, 2021, **11**(1), 22668.
58 M. D. A. Norman, S. A. Ferreira, G. M. Jowett, L. Bozec and E. Gentleman, Measuring the elastic modulus of soft culture surfaces and three-dimensional hydrogels using atomic force microscopy, *Nat. Protoc.*, 2021, **16**(5), 2418–2449.
59 A. M. Smith, D. G. Inocencio, B. M. Pardi, A. Gopinath and R. C. Andresen Eguiluz, Facile determination of the Poisson's ratio and Young's modulus of polyacrylamide gels and polydimethylsiloxane, *ACS Appl. Polym. Mater.*, 2024, **6**(4), 2405–2416.
60 P. Eliahoo, H. Setayesh, T. Hoffman, Y. Wu, S. Li and J. B. Treweek, Viscoelasticity in 3D cell culture and regenerative medicine: measurement techniques and biological relevance, *ACS Mater. Au*, 2024, **4**(4), 354–384.
61 H. N. Qiu, J. Lin, L. X. Hou, R. Xiao, Q. Zheng and Z. L. Wu, Stress relaxation and creep response of glassy hydrogels with dense physical associations, *ACS Appl. Mater. Interfaces*, 2025, **17**(6), 9981–9991.
62 B. A. Nerger, K. Kashyap, B. T. Deveney, J. Lou, B. F. Hanan, Q. Liu, A. Khalil, T. Lungjangwa, M. Cheriyan, A. Gupta, R. Jaenisch, D. A. Weitz, L. Mahadevan and D. J. Mooney, Tuning porosity of macroporous hydrogels enables rapid rates of stress relaxation and promotes cell expansion and migration, *Proc. Natl. Acad. Sci. U. S. A.*, 2024, **121**(45), e2410806121.
63 C. Huerta-López, A. Clemente-Manteca, D. Velázquez-Carreras, F. M. Espinosa, J. G. Sanchez, Á. Martínez-Del-Pozo, M. García-García, S. Martín-Colomo, A. Rodríguez-Blanco, R. Esteban-González, F. M. Martín-Zamora, L. I. Gutierrez-Rus, R. Garcia, P. Roca-Cusachs, A. Elosegui-Artola, M. A. Del Pozo, E. Herrero-Galán, P. Sáez, G. R. Plaza and J. Alegre-Cebollada, Cell response to extracellular matrix viscous energy dissipation outweighs high-rigidity sensing, *Sci. Adv.*, 2024, **10**(46), eadf9758.
64 M. Pittman, E. Iu, K. Li, M. Wang, J. Chen, N. Taneja, M. H. Jo, S. Park, W.-H. Jung, L. Liang, I. Barman, T. Ha, S. Gaitanaros, J. Liu, D. Burnette, S. Plotnikov and Y. Chen, Membrane ruffling is a mechanosensor of extracellular fluid viscosity, *Nat. Phys.*, 2022, **18**(9), 1112–1121.
65 A. Amitrano, Q. Yuan, B. Agarwal, A. Sen, Y. W. Dance, Y. Zuo, J. M. Phillip, L. Gu and K. Konstantopoulos, Extracellular fluid viscosity regulates human mesenchymal stem cell lineage and function, *Sci. Adv.*, 2025, **11**(1), eadr5023.
66 P. Sacco, F. Piazza, C. Pizzolitto, G. Baj, F. Brun, E. Marsich and I. Donati, Regulation of substrate dissipation *via*

tunable linear elasticity controls cell activity, *Adv. Funct. Mater.*, 2022, **32**(29), 2200309.
67 J. Xie, M. Bao, X. Hu, W. J. H. Koopman and W. T. S. Huck, Energy expenditure during cell spreading influences the cellular response to matrix stiffness, *Biomaterials*, 2021, **267**, 120494.
68 H. Eslami and A. Darvishi, Extracellular matrix viscoelasticity: a dynamic regulator of cellular behavior, *Ann. Biomed. Eng.*, 2025, **53**(9), 2029–2046.
69 S. Scott, M. Villiou, F. Colombo, A. D. la Cruz-García, L. Tydecks, L. Toelke, K. Siemsen and C. Selhuber-Unkel, Dynamic and reversible tuning of hydrogel viscoelasticity by transient polymer interactions for controlling cell adhesion, *Adv. Mater.*, 2025, **37**(12), e2408616.
70 E. E. Charrier, K. Pogoda, R. G. Wells and P. A. Janmey, Control of cell morphology and differentiation by substrates with independently tunable elasticity and viscous dissipation, *Nat. Commun.*, 2018, **9**(1), 449.
71 F. Chen, W. Z. Sun, F. Mokhtari-Esbuie, Z. Moghimi, M. F. I. Chowdhury, A. Yazdani, J. W. Harmon and G. Sun, Responsive gelatin-hyaluronic acid hydrogel scaffold boosting antioxidant activity for enhanced diabetic wound healing, *Appl. Mater. Today*, 2025, **44**(102752), 102752.
72 K. C. M. L. Elvitigala, W. Mubarok and S. Sakai, Tuning the crosslinking and degradation of hyaluronic acid/gelatin hydrogels using hydrogen peroxide for muscle cell sheet fabrication, *Soft Matter*, 2023, **19**(31), 5880–5887.
73 M. Zhang, Q. Ye, Z. Zhu, S. Shi, C. Xu, R. Xie and Y. Li, Hyaluronic acid-based dynamic hydrogels for cartilage repair and regeneration, *Gels*, 2024, **10**(11), 703.
74 A. Bauer, L. Gu, B. Kwee, W. A. Li, M. Dellacherie, A. D. Celiz and D. J. Mooney, Hydrogel substrate stress-relaxation regulates the spreading and proliferation of mouse myoblasts, *Acta Biomater.*, 2017, **62**, 82.
75 G. M. Gathman, M. M. Patel, D. I. Walter and R. S. Stowers, Matrix viscoelasticity regulates dermal fibroblast activation in a three-dimensional fibrillar microenvironment, *bioRxiv*, 2026, DOI: 10.64898/2026.03.02.709111.
76 C. Liu, Q. Yu, Z. Yuan, Q. Guo, X. Liao, F. Han, T. Feng, G. Liu, R. Zhao, Z. Zhuang, H. Mao, C. Zhu and B. Li, Engineering the viscoelasticity of gelatin methacryloyl (GelMA) hydrogels via small ''dynamic bridges'' to regulate BMSC behaviors for osteochondral regeneration, *Bioact. Mater.*, 2023, **25**, 445.
77 M. Lekka, K. Gnanachandran, A. Kubiak, T. Zieliński and J. Zemła, Traction force microscopy - measuring the forces exerted by cells, *Micron*, 2021, **150**, 103138.
78 M. Goktas and K. G. Blank, Molecular force sensors: from fundamental concepts toward applications in cell biology, *Adv. Mater. Interfaces*, 2017, **4**(1), 1600441.
79 A. M. Obenaus, M. Y. Mollica and N. J. Sniadecki, De-form and function: measuring cellular forces with deformable materials and deformable structures, *Adv. Healthc. Mater*, 2020, **9**(8), 1901454.
80 B. Cheng, M. Li, M. Lin, H. Guo and F. Xu, Mechanobiology across timescales, *Nat. Rev. Phys.*, 2025, **7**(11), 621–644.
81 Z. Zhang, P. He, L. Yang, J. Gong, R. Qin and M. Wang, Posttranslational modifications of YAP/TAZ: molecular mechanisms and therapeutic opportunities, *Cell. Mol. Biol. Lett.*, 2025, **30**(1), 83.
82 F.-X. Yu, B. Zhao, N. Panupinthu, J. L. Jewell, I. Lian, L. H. Wang, J. Zhao, H. Yuan, K. Tumaneng, H. Li, X.-D. Fu, G. B. Mills and K.-L. Guan, Regulation of the Hippo-YAP pathway by G-protein-coupled receptor signaling, *Cell*, 2012, **150**(4), 780–791.
83 C. G. Hansen, T. Moroishi and K.-L. Guan, YAP and TAZ: a nexus for hippo signaling and beyond, *Trends Cell Biol.*, 2015, **25**(9), 499–513.
84 M. Fu, Y. Hu, T. Lan, K.-L. Guan, T. Luo and M. Luo, The Hippo signalling pathway and its implications in human health and diseases, *Signal Transduct. Target. Ther.*, 2022, **7**(1), 376.
85 J. Chen, J. Zhang, Y. Zhu, Y. Zhu, J. Pang, Q. Wu, Y. Wang and Q. Zhan, Focal adhesion kinase/src family kinase axis-mediated tyrosine phosphorylation of metabolic enzymes facilitates tumor metastasis, *Signal Transduct. Target. Ther.*, 2025, **10**(1), 280.
86 M. Ritt, J. L. Guan and S. Sivaramakrishnan, Visualizing and manipulating focal adhesion kinase regulation in live cells, *J. Biol. Chem.*, 2013, **288**(13), 8875–8886.
87 Z. S. Wilson, H. Witt, L. Hazlett, M. Harman, B. M. Neumann, A. Whitman, M. Patel, R. S. Ross, C. Franck, J. S. Reichner and C. T. Lefort, Context-dependent role of vinculin in neutrophil adhesion, motility and trafficking, *Sci. Rep.*, 2020, **10**(1), 2142.
88 M. R. Chastney, J. Kaivola, V.-M. Leppänen and J. Ivaska, The role and regulation of integrins in cell migration and invasion, *Nat. Rev. Mol. Cell Biol.*, 2025, **26**(2), 147–167.
89 M. Hałas-Wiśniewska, P. Zawadka, W. Arendt and M. Izdebska, From adhesion to invasion: integrins, focal adhesion signaling, and actin binding proteins in cervical cancer progression-a scoping review, *Cells*, 2025, **14**(20), 1640.
90 M. Vázquez-González and I. Willner, Stimuli-responsive biomolecule-based hydrogels and their applications, *Angew. Chem., Int. Ed.*, 2020, **59**(36), 15342–15377.
91 J. S. Kahn, Y. Hu and I. Willner, Stimuli-responsive DNA-based hydrogels: from basic principles to applications, *Acc. Chem. Res.*, 2017, **50**(4), 680–690.
92 M. Fadeev, G. Davidson-Rozenfeld, Z. Li and I. Willner, Stimuli-responsive DNA-based hydrogels on surfaces for switchable bioelectrocatalysis and controlled release of loads, *ACS Appl. Mater. Interfaces*, 2023, **15**(30), 37011–37025.
93 Z. Li, G. Davidson-Rozenfeld, M. Vázquez-González, M. Fadeev, J. Zhang, H. Tian and I. Willner, Multi-triggered supramolecular DNA/bipyridinium dithienylethene hydrogels driven by light, redox, and chemical stimuli for shape-memory and self-healing applications, *J. Am. Chem. Soc.*, 2018, **140**(50), 17691–17701.
94 R. Baretta, G. Davidson-Rozenfeld, V. Gutkin, M. Frasconi and I. Willner, Chemical and photochemical-driven dissipative Fe^{3+}/Fe^{2+}-ion cross-linked carboxymethyl cellulose gels operating under aerobic conditions: applications for transient controlled release and mechanical actuation, *J. Am. Chem. Soc.*, 2024, **146**(14), 9957–9966.

95 G. Davidson-Rozenfeld, X. Chen, Y. Qin, Y. Ouyang, Y. S. Sohn, Z. Li, R. Nechushtai and I. Willner, Stiffness-switchable, biocatalytic pH-responsive DNA-functionalized polyacrylamide cryogels and their mechanical applications, *Adv. Funct. Mater.*, 2024, **34**(4), 2306586.

96 K. Yin, K. Ji, L. S. Littles, R. Trivedi, A. Karma and U. G. K. Wegst, Hierarchical structure formation by crystal growth-front instabilities during ice templating, *Proc. Natl. Acad. Sci. U. S. A.*, 2023, **120**(23), e2210242120.

97 W. Gu, S. Yang, D. Zhao, Y. Zou, C. Chen, P. Niu, X. Liang, C. T. Kwok, B. Zhou, C. Wang, Y. Y. S. Huang, J. Liu and I. M. Lei, Concentric ice-templating of ultracompressible tough hydrogels with bioinspired circumferentially aligned architecture, *Sci. Adv.*, 2025, **11**(25), eadv7786.

98 T. Hu, M. Shi, X. Zhao, Y. Liang, L. Bi, Z. Zhang, S. Liu, B. Chen, X. Duan and B. Guo, Biomimetic 3D aligned conductive tubular cryogel scaffolds with mechanical anisotropy for 3D cell alignment, differentiation and in vivo skeletal muscle regeneration, *Chem. Eng. J.*, 2022, **428**(131017), 131017.